Chemosphere 338 (2023) 139576

Contents lists available at ScienceDirect

Chemosphere

journal homepage: www.elsevier.com/locate/chemosphere

Photocatalytic fixation of NO_x in soils

Antonio R. Sánchez-Rodríguez [a], Elena Gómez-Álvarez [a], José M. Méndez [a], Ute M. Skiba [b], Davey L. Jones [c,d], Dave R. Chadwick [d], María C. del Campillo [a], Raphael BA. Fernandes [e], Jörg Kleffmann [f], Vidal Barrón [a,*]

[a] Department of Agronomy, Universidad de Córdoba, 14071, Córdoba, Spain
[b] UK Centre for Ecology & Hydrology, Edinburgh, UK
[c] Food Futures Institute, Murdoch University, WA 6105, Perth, Australia
[d] School of Natural Sciences, Bangor University, UK
[e] Department of Soil Science, Universidade Federal de Viçosa, MG, Brazil
[f] Department of Physical and Theoretical Chemistry, Faculty for Mathematics and Natural Sciences, University of Wuppertal, 42097, Wuppertal, Germany

HIGHLIGHTS

- Photocatalytic NO_x fixation by soils could be a mechanism to reduce air pollution.
- Low Ti oxides (<5%) in some soils match pure TiO_2 for photocatalysis.
- Atmospheric models should include this abiotic renoxification route.
- This mechanism could be a source of NO_3^- for plants.
- Sustainable strategies in agriculture could benefit from NOx fixation by soils.

GRAPHICAL ABSTRACT

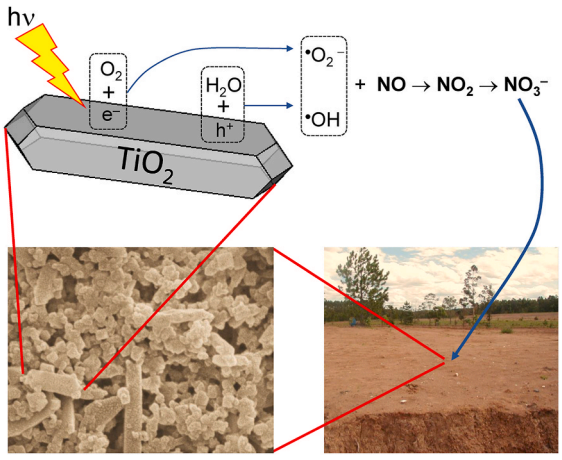

ARTICLE INFO

Handling editor: Sergi Garcia-Segura

Keywords:
NO_x fixation
Natural photocatalysis
Anatase
Rutile
Iron oxides

ABSTRACT

Nitrogen oxides (NO_x = NO + NO_2) are important atmospheric pollutants that are directly harmful to human health. Recently in urban and industrial areas, synthetic materials have been developed and deployed to photocatalytically oxidize NO_x to nitrate (NO_3^-) in order to improve air quality. We show that the natural presence of small amounts (≤5%) of titanium oxides, such as anatase and rutile, can also drive NO_x oxidation to nitrate in soils under UV–visible irradiation. The NO uptake coefficients ranged between 0.1×10^{-6} for sandy soils to 6.4×10^{-5} in the case of tropical clay soils; the latter comparable in efficiency to current industrial man-made catalysts. This photocatalytic *N*-fixation mechanism offers a new strategy for NO_x mitigation from the

* Corresponding author.
E-mail address: vidal@uco.es (V. Barrón).

https://doi.org/10.1016/j.chemosphere.2023.139576
Received 19 May 2023; Received in revised form 4 July 2023; Accepted 17 July 2023
Available online 18 July 2023

atmosphere by transforming it into nitrate, and simultaneously provides an energy efficient source of essential fertilizer to agriculture.

1. Introduction

Soils are essential components of terrestrial ecosystems, being a medium for plant and microbial growth, element and organic matter cycling, landscaping and engineering, and a regulator of water supplies (Bünemann et al., 2018; Banwart et al., 2019). The role of soil in atmospheric gas exchange is well recognized: fixing CO_2 into the soil through plants and sequestering C as humus, generating CH_4, H_2S and N_2O in anaerobic soil processes, and from emissions of nitrogen oxides (NO_x) through nitrification and denitrification processes. While biotic soil emissions of nitrogen oxides ($NO_x = NO + NO_2$) have been intensively studied in the past and algorithms for models established (Pilegaard, 2013), research addressing abiotic emission and fixation of NO_x in soils is scarce (Doane, 2017a; Barrón et al., 2020). This is surprising since nitrogen oxides are important components of the atmosphere (as precursors of ozone, photochemical smog, acid rain, particles) and their oxidized product nitric acid an important soil nutrient. In particular, NO_2 is directly harmful to human health, animals and plants. Atmospheric NO_x originates predominantly from anthropogenic sources namely combustion of fossil fuels and agriculture, with smaller contributions from lightning and biomass burning, highest ambient concentrations being found in and downwind of highly populated megacities (Guo et al., 2020).

Various abatement strategies have been explored to minimize their concentration in the atmosphere in highly populated regions. One such mitigation strategy is through heterogeneous photocatalysis which drives the oxidation of NO to nitrate (NO_3^-) (Laufs et al., 2010; Russell et al., 2021). This involves construction and urban deployment of synthetic semiconducting materials including Bi-based materials, graphite phase carbon nitride (g-C_3N_4) (Li et al., 2022), layered double hydroxide (Fragoso et al., 2023), α-Fe_2O_3, ZnO, pure or combined with additives such as clay, carbon or mesoporous materials and specially TiO_2-related materials, which catalyze these reactions (Balbuena et al., 2015). These semiconducting materials are applied to surfaces, for example in paints or coatings (Gandolfo et al., 2015), and activated by light, preferably UV because its energy is similar or greater than that of the band gap between the conduction and the valence band. This mechanism creates electrons and holes in the semiconductor. By consecutive reactions with H_2O/OH^- and O_2 reactive oxygen species (ROS) are generated, such as $^{\bullet}O_2^-$ and $^{\bullet}OH$ radicals (Georgiou et al., 2015). These radicals transform NO into nitrates, passing through intermediate species such as NO_2 (Laufs et al., 2010).

Enormous financial and research resources have been employed to enhance the photocatalytic performance of synthetic materials and to characterize by-products (Russell et al., 2021). However, natural soils containing similarly photocatalytically active compounds could offer a much more cost-effective and sustainable solution to NO_x mitigation than the usual synthetic compound approach. An assessment of these unexplored reactions in globally representative soils is needed to determine the variability observed in soil NO_x emissions from agricultural soils under illumination (Guo et al., 2020).

In this work, we report on a series of experiments focused on light induced photocatalytic reactions of NO with twenty-four soils from around the world, differing in color, particle size distribution, soil properties (mainly organic matter and nitrogen contents) and mineralogy. First, we evaluate the ability of agricultural soils to uptake atmospheric NO abiotically, i.e., their photocatalytic efficiency. Second, we determine the formation of nitrate, i.e., the photocatalytic fertilization of soils, and third, we identify the main soil components involved in these reactions and assess their contribution. Using different dissolution treatments to selectively remove organic matter, iron oxides (hematite and/or goethite) or aluminium hydroxide (gibbsite) we revealed that Ti oxides (anatase and rutile), with concentrations below 5%, are the key photocatalytic minerals and that Fe oxide pigments, especially hematite, not only do not improve photocatalytic efficiency but can mask the action of Ti oxides. Interestingly, for well weathered goethitic/hydromorphic soils, NO reduction values comparable to those of pure TiO_2 can be achieved.

2. Materials and methods

2.1. Soils

This study was carried out with samples of 24 different soils, mainly from Spain and Brazil, and, also, two soils from Italy and Great Britain. They included, according to the FAO-Unesco system (WRB, 2015): cambisols, calcisol, luvisols, acrisol, vertisols and ferralsols, which were collected from either A or B horizons (Table S1). The soil samples were air-dried, sieved to 2 mm and analyzed for particle size distribution (sand, silt and clay fractions) with the pipette method (Gee and Bauder, 1986) and organic matter with the Walkley-Black method (Nelson and Sommers, 1982). The specific surface area was determined by H_2O adsorption at 20% relative humidity (Quirk, 1955). Samples for soluble total N and NO_3^- analysis were extracted with 0.5 M K_2SO_4 at a soil: solution ratio of 1:5. Total N and nitrate were analyzed by a nitrogen analyzer with a chemiluminescent detector (Shimadzu TNM-L) and by spectrophotometry on a Power-Wave-HT (Biotek) microplate reader (Mulvaney, 1996) respectively. Well crystallized mineral phases were identified and quantified from the grounded and sieved <0.5 mm soil sample by: (a) elemental chemical analysis from X-ray fluorescence (XRF) using a Rigaku ZSK PrimusIV wavelength X-ray spectrometer. The system was equipped with a 3 kW Rh-target X-ray tube, ten analyzer crystal, a sealed proportional counter for light elements detection and a scintillation counter for heavy elements; and (b) X-ray diffraction (XRD) (Whittig and Allardice, 1986) on a Bruker D8 Advance instrument using monochromatized Cu K radiation (Figures S1a-c). Key minerals as Ti and Fe oxides at low contents could not be estimated directly from the powder of the natural soil. Therefore, the concentration of anatase and rutile (no other Ti phases were identified) was obtained also from XRD, but after they were concentrated removing iron oxides selectively by using DCB (Mehra and Jackson, 1960) and silicates with HF–HCl treatment (Raman and Jackson, 1965). From the diffraction peak broadening for the main reflections for anatase and rutile the crystallite size of these phases was determined by means of the Scherrer equation (Klugg and Alexander, 1974). This equation was calculated with DIFFRACT. EVA V3.1 software (Bruker). Furthermore, the size and morphology of the samples were examined by transmission electron microscopy (TEM) using a JEOL JEM 1400 and scanning electron microscopy (SEM) using a JEOL JSM-7800F6400 instrument. Hematite and goethite were quantitatively analyzed from a) the content of free Fe as determined by DCB extractant (Mehra and Jackson, 1960), and b) from the second derivative of the visible spectra of fine powder (Scheinost et al., 1998), recording them on a Cary 5000 spectrophotometer equipped with diffuse reflectance accessory (Figures S2a-c). Ferrimagnetic phases (magnetite/maghemite) were estimated from the low frequency magnetic susceptibility measurements using a MS2 Bartington susceptibility meter.

2.2. Photocatalytic experiments

The photocatalytic activity of the soils was quantified as uptake coefficients (see below) from the amount of NO removed from a constant

airflow of NO (~100 ppb) in humidified synthetic air passing through a bed-flow photoreactor. The reactor is equipped with a quartz window transparent to UV and visible light (Figure S3) and with a sample holder of 5 cm × 5 cm (geometric surface area 25 cm^2) and 0.3 cm depth. The amount of air-dried soil sample (>8 g mass corresponding to the 0.3 cm thickness) was sufficiently high to ensure the maximum NO fixation (Figure S4). In fact, only below 0.1 cm (about 2 g) a sharp decrease in NO fixation was observed. The NO-air gas mixture was passed over the soil sample (the distance between the quartz window and the soil sample was 3 mm). Both in the atmosphere and in the reactor, NO will react mainly with the top layer, but some passive diffusion into the bulk will also take place. For simplicity, the uptake coefficient is calculated by the geometric surface area (see Eq. (1) below), but it depends on the true surface area, and hence on the NO diffusion into the bulk of the soil. Thus, the reported numerical values will overestimate the true uptake coefficients and will partly scale with the mass of the soil for thin soil layers. The uptake coefficient determined in this study correspond to the experimental conditions and were calculated to rank the different soils.

Either filtered compressed external air or synthetic air (Linde) were passed at a flow rate of 400 ml/min through a washing bottle at 25 ± 2 °C filled with demineralized water. This was mixed with 200 ml of dry air resulting in 70% RH. The reactor temperature was fixed to 20±1 °C with a Peltier thermoelectric cooler device.

The photoreactor was placed inside a light-sealed irradiation box (Solarbox 3000e). A Xenon lamp with irradiance control and an irradiation spectrum comparable to solar radiation provided the energy to induce photocatalysis. Solarbox 3000e was calibrated by manufacturer using internal company procedures developed in accordance to UNI EN 9000 specifications. The installed UV filter used in the experiments was S305 outdoor (Figure S3). The nominal irradiance value (290–800 nm) in position 7 (used for most of the experiments), i.e. was irradiances of 27 (UV) and 550 (VIS) W m^{-2}. Only for the experiment where the balance of the transformation of NO_x to NO_3^- was investigated (Table S2), irradiances of 35 (UV) and 620 (Vis) W m^{-2} were applied.

Nitrogen oxide concentrations (NO and NO_2) were monitored using a chemiluminescence analyzer (Environnement AC32 M). Interferences against other reactive nitrogen species (NO_y) in the NO_x channel of the instrument (Villena et al., 2012) were not considered here. Thus, NO_2 concentrations will be overestimated and reflect the sum of NO_2 and other NO_y species, for example nitrous acid (HONO). Passing the air/NO gas stream over the sample in the dark for 10 min caused no change in the NO concentration profiles, thus ruling out potential NO adsorption or dark reaction onto the sample surface. Subsequently, the photoreactor was irradiated for 60 min.

The uptake coefficients (γ_{geo}) of NO were calculated according to the following equation (Pill et al., 2021):

$$\gamma_{geo} = \frac{4 \times \varphi_g \times ln\left(\frac{c_{t=0}}{c_t}\right)}{\overline{\upsilon} \times S_{geo}} \quad (1)$$

Where, φ_g is the gas flow rate (10 cm^3 s^{-1}), $c_{t=0}$ and c_t are the NO mixing ratios [ppb] at the inlet and exit of the photoreactor, respectively, S_{geo} is the geometric surface area (25 cm^2) of the sample, and $\overline{\upsilon}$ the mean velocity of the reactants (cm s^{-1}) according to the gas kinetic theory ($\overline{\upsilon} = (8 \times R \times T \times \pi^{-1} \times M^{-1})^{0.5} \times C$, with: R = 8.314 J mol^{-1} K^{-1}, T = absolute temperature (293 K), M = molar mass of 0.030 kg mol^{-1} for NO and C = 100 cm m^{-1}).

γ_{geo} is a simple and useful parameter for atmospheric modelling since it does not require to know any additional parameters such as pore size or distribution, which would unnecessarily complicate the estimation of gaseous uptakes on porous and highly complicated surfaces as is the case for soils.

Some concepts have been used to describe pore diffusion/uptake, e.g. the pore diffusion model (Keyser et al., 1991). The use of true uptake coefficient (γ_{true}) for which the physical surface accessed by the reactant is used is trivial for flat, non-porous surfaces for which the true surface is similar to the geometric surface area. However, applying γ_{true} adds significant complexity in the case of porous surfaces like soils since it requires a previous knowledge of the size distribution of the pores in the soil. The depth the molecules diffuse into the bulk and the internal surface need to be known, for which typically the BET surface is used. To determine γ_{true} the mass of the substrate (i.e., the soil) is increased in the low range for which the first order rate coefficient increases linearly with the soil mass. Under these conditions the mass and the BET surface are used to calculate the total surface area that NO can access from which γ_{true} is determined. However, with increasing mass – as is the case in the real environment -, the first order rate coefficient deviates from linearity and gets constant at a given soil mass/thickness of the soil layer when the amount of reactant removed by heterogeneous uptake, while diffusing through the soil pores levels off. Under these conditions, the maximum uptake is obtained, which will be similar to that on real bulk soil surfaces in the environment.

When describing the heterogeneous uptake on ground surfaces in a model, the concept of the deposition velocity (ν) is typically used. The flux to the surface (geometric surface used in atmospheric models) is described by a resistance model, which depends on the turbulent mixing of the lower atmosphere (described by the resistance R_a), the quasi-molecular diffusion near the surface (R_b) and the heterogeneous uptake on the surface (described by the surface resistance, R_c). While R_a and R_b can be parameterized by micro-meteorological concepts, R_c is determined from uptake data from the lab. Here, the inverse of R_c is directly proportional to the geometric uptake coefficient (γ_{geo}), which is used in the present study for soil mass independent conditions. Hence, increasing the amount of soil will not result in an increase of the amount of NO reacting with it. In our experiments the soil layer was thick enough that all NO reacted during the pore diffusion in the soil bed used. Thus, the first order rate coefficients are independent of the soil mass and will be similar to the real environment independently of how large the accessed true surface area is in reality. This quantity is more relevant for describing photocatalytic uptake on soil surfaces in the environment than the more theoretical quantity of γ_{true} described above. Photocatalytic experiments were carried out using three replicates for each of the twenty-four soils. Additionally, we also evaluated the photocatalytic activity of soils after: 1) removing Fe oxides with DCB (Mehra and Jackson, 1960); 2) destroying organic matter with H_2O_2 (Gee and Bauder, 1986), and 3) dissolving Al hydroxide (gibbsite) by boiling for 1 h in 5 M NaOH (Kampf and Schwertmann, 1982). After each of the three independent treatments to remove Fe oxides, organic matter and Al hydroxide the samples were subsequently washed four times with 0.5 M K_2SO_4, twice with deionized water and were finally oven-dried at 60 °C. A similar procedure to 2) with an additional washing step with K_2SO_4, and deionized water was applied for the determination of the balance of nitrates, ensuring the complete removal of total nitrates before photocatalytic experiment, which was tested according to Mulvaney (1996).

2.3. Statistical analysis

A Principal Component Analysis (PCA) was conducted to assess the main soil components and properties that were related to NO_x fixation in natural soils and soils after removing Fe/Al oxihydroxides or organic matter content. The PCA was performed using R' software (R Core Team, 2020) and the packages: "FactoMineR", "ade4", "ExPosition", "Hmisc" and "ggplot2". Additionally, Pearson correlations were done between the different soil variables measured before the photocatalytic experiments and NO uptake.

3. Results and discussion results

3.1. Soil properties

The organic matter content of the soils (Table 1) was not higher than

Table 1
Selected properties and composition of soils used in this study.

Sample	Organic Matter	Soluble total N	$N–NO_3^-$	Texture			Surface area	pH	Minerals										
				Clay	Silt	Sand			Quartz	Feldspar	Mica-illite	Vermic.-Chlorite	Kaolinite	Smectite	Calcite	Gibbsite	Hematite	Goethite	Magn.+ maghemite
	%	mg kg^{-1}		%			m^2 g^{-1}		%										
CAM1	1.6	61.5	16.6	12	2	86	26.3	6.5	38	39	16	0	4	0	0	0	0.03	0.33	0.03
POZ1	3.7	186.6	53.1	15	12	73	52.4	7.6	35	36	20	0	4	0	0	0	0.02	0.32	0.03
DAV1	4.9	66.3	6.6	28	12	60	84.1	6.0	40	17	15	5	15	0	0	0	0.26	1.21	0.11
CPN1	1.2	47.6	0.6	71	8	21	340.2	8.0	17	0	5	0	5	64	6	0	0.27	0.45	0.06
RAB1	3.5	81.8	11.5	50	40	10	52.1	7.8	30	0	12	0	4	34	15	0	0.02	0.47	0.04
MON2	0.4	21.0	9.1	58	12	30	130.9	6.7	36	10	30	0	20	0	0	0	1.26	1.29	0.20
IAS1	1.0	26.6	4.7	21	44	35	53.8	8.4	29	20	18	1	0	4	25	0	0.34	0.30	0.05
ACR1	2.2	11.5	0.0	4	10	86	22.8	6.9	67	0	28	0	1	0	0	0	0.36	0.35	0.06
MNL1	1.2	25.8	0.1	32	15	53	71.8	8.1	46	5	19	0	12	0	15	0	0.26	0.72	0.08
IN20	1.8	35.2	4.1	17	72	11	53.1	8.8	9	5	5	0	5	3	70	0	0.13	0.19	0.03
PUEZ	1.4	46.9	20.2	65	9	27	183.9	8.1	30	0	15	0	49	0	0	0	2.79	0.56	0.28
FTPZ	1.3	22.0	2.6	28	7	65	79.5	8.8	60	0	18	0	18	0	0	0	0.72	0.48	0.10
RF01	1.9	68.5	14.9	43	20	37	59.2	5.7	35	0	0	0	8	0	0	30	12.81	6.03	1.54
RF02	0.5	26.0	0.6	28	12	60	28.0	5.1	34	0	0	0	10	0	0	30	16.91	3.22	1.67
MES2	2.5	71.8	1.3	53	6	42	62.8	4.7	33	0	0	0	39	0	0	15	7.10	1.61	0.72
QT32	0.8	17.6	0.9	59	5	36	126.0	7.4	49	0	0	0	45	0	0	0	0.61	3.66	0.33
MES3	3.6	97.5	0.6	78	3	20	70.8	5.0	24	0	0	0	21	0	0	35	7.14	5.64	1.03
JVM2	1.2	19.8	0.7	40	17	44	100.8	5.3	5	0	0	0	5	0	0	56	22.73	2.48	2.11
RF06	0.9	64.1	14.9	83	12	5	91.3	4.4	20	0	5	0	18	0	0	50	0.05	4.54	0.35
JVM6	1.2	35.8	0.1	65	12	24	46.2	4.6	35	0	0	0	47	0	0	5	0.09	8.65	0.66
MES6	2.0	67.9	5.5	90	2	9	62.6	4.7	10	0	0	0	20	0	0	57	0.08	7.99	0.61
RF22	1.1	45.7	4.2	67	6	27	50.2	4.5	20	0	5	0	19	0	0	40	2.70	9.59	0.96
RF16	1.9	43.5	0.8	86	9	5	60.2	5.2	16	0	0	0	10	0	0	63	0.05	4.72	0.36
RF10	2.1	33.2	0.7	75	14	11	82.4	5.5	15	0	0	0	10	0	0	54	0.14	13.80	1.06
MIN	0.4	11.5	0.0	4.0	1.7	5.0	22.8	4.4	5.0	0.0	0.0	0.0	0.0	0.0	0.0	0.0	0.0	0.2	0.0
MAX	4.9	186.6	53.1	89.8	72.0	86.0	340.2	8.8	67.0	39.0	30.0	5.0	49.0	64.0	70.0	63.0	22.7	13.8	2.1
Average	1.8	51.0	7.3	48.6	15.0	36.4	83.0	6.4	30.5	5.5	8.8	0.3	16.2	4.4	5.5	18.1	3.2	3.3	0.5

5%, as it is typical for many temperate and tropical soils (Weil and Brady, 2016; Lal, 2020). Some of the highest concentrations of soluble total N (186.6 mg kg^{-1}, POZ1) and $N–NO_3^-$ (53.1 mg kg^{-1}, DAV1) also corresponded to high organic matter values or a recent nitrogen fertilization event (e.g. PUEZ). Textural classes ranged from loamy sand to clay (Table 1, Figure S5), with a wide variation in clay content (4–89%) and surface area (23–340 m^2 g^{-1}). Soil pH also widely varied from 4.4 for tropical soils to 8.8 for temperate calcareous soils. Mineral composition (Table 1, Figures S1a-c) was consistent with their different parent materials and the climatic zones where they have formed (Table S1). Quartz was present in all soils and was dominant in the sandy soils, which also contained significant amounts of feldspars. Felspars were absent in tropical soils (RF, MES and JVM samples), where phyllosilicates such as kaolinite were very common. Other phyllosilicates as mica or illite were also present in the rest of the soils. Smectite was the major clay mineral in soils developed on marls under Spanish Mediterranean climate, where also calcite was present (CPN1, RAB1). In agreement with Barrón and Torrent (2013) gibbsite together with Fe oxides (especially hematite and goethite) were in high content in the highly weathered tropical samples. These Fe oxides were mainly responsible for the red and yellow pigmentation (from 3 YR to 9.1 YR Munsell hues (Torrent and Barrón, 1993)) exhibited by the soils (Figures S2a-c). Ti oxides appeared in all samples at concentrations below 5% (Table 2); the highest values also corresponded to intensely weathered soils, typical from tropical climates (Fitzpatrick and Chittleborough, 2018). Due to the low TiO_2 concentration of some samples (15 of them had less than 1%), it was only possible to identify and quantify the different phases by X-ray diffraction after a selective dissolution of silicates using a strong HF–HCl treatment followed by removal of iron oxides with dithionite-citrate-bicarbonate (DCB). After this procedure other phases sporadically present in soils, e.g. brookite, ilmenite or titanite, were not found, and only anatase (An) and rutile (Rt) were identified (Figures S1a-c, inset); the An/(An + Rt) ratio ranged between 0.2 and 0.9 (Table 2). As is typical, the most common forms of Ti in soils are residual rutile, inherited from weathering of bed-rock, or neoformed anatase (Fitzpatrick and Chittleborough, 2018). Transmission and scanning electron microscope observations for sample FTPZ showed that most anatase (pellets) and rutile (sticks) were <500 nm in size (Fig. 1).

This sub-micrometric grain size (clay fraction) for Ti oxides in natural environments has also been found by other authors (Raman and Jackson, 1965; Fitzpatrick et al., 1978; Pradas del Real et al., 2018). Consistent with these images we found for all samples that the mean crystallite size, derived from the X-ray diffraction peak broadening (analyzed from the concentrated TiO_2 phases after HF–HCl-DCB treatment for removing silicates and iron oxides), ranged from 53 to 308 nm for anatase and from 44 to 972 nm for rutile (Table 2).

Table 2
Characteristics of the TiO_2 phases in the soils used in this study.

Sample	TiO_2	Anatase	Rutile	Anat/(Anat + Rut)	Crystal Size Anatase	Crystal Size Rutile
	%				nm	
CAM1	0.39	0.26	0.13	0.66	68	112
POZ1	0.43	0.30	0.12	0.71	57	70
DAV1	0.65	0.12	0.52	0.19	296	178
CPN1	0.38	0.16	0.23	0.41	116	188
RAB1	0.55	0.36	0.19	0.66	308	150
MON2	0.73	0.39	0.33	0.54	102	75
IAS1	0.47	0.20	0.27	0.42	203	100
ACR1	0.73	0.49	0.24	0.67	79	95
MNL1	0.50	0.18	0.33	0.35	185	972
IN20	0.12	0.05	0.07	0.44	103	120
PUEZ	0.54	0.37	0.17	0.68	84	149
FTPZ	0.47	0.19	0.28	0.41	143	67
RF01	3.97	3.18	0.79	0.80	63	44
RF02	3.57	2.67	0.89	0.75	145	131
MES2	0.78	0.46	0.32	0.59	165	93
QT32	0.36	0.19	0.18	0.51	63	64
MES3	1.68	0.84	0.84	0.50	95	108
JVM2	4.81	4.42	0.38	0.92	59	68
RF06	0.76	0.40	0.36	0.53	74	49
JVM6	1.55	1.10	0.45	0.71	53	161
MES6	1.74	0.87	0.87	0.50	117	123
RF22	1.17	0.96	0.21	0.82	55	825
RF16	3.76	2.56	1.20	0.68	105	121
RF10	3.53	2.19	1.34	0.62	126	165
MIN	0.12	0.05	0.07	0.19	53	44
MAX	4.81	4.42	1.34	0.92	308	972
Average	1.40	0.95	0.45	0.59	119	176

3.2. Photocatalytic abatement of NOx in soils and nitrate formation

The concentration of gaseous nitric oxide (NO) (Fig. 2, blue line) that flowed over the soil sample was set at 100 ppb (representative of typical NO_x levels in many urban and freshly fertilized agricultural environments) which decreased dramatically (depending on the soil) when the light was turned on. It is important to note that the UV–visible lamp used does not produce ozone or H_2O_2, irradiating in the wavelength range 290–800 nm, (see Photocatalytic Experiments). For the next 60 min under UV–Visible radiation, the gaseous NO was partially oxidized by natural photocatalysis to nitrogen dioxide (NO_2). Some components of the natural soil, such as TiO_2, are clearly able to photocatalytically oxidize NO analogously to the synthetically developed systems. The small concentrations of NO_2 thus generated (Fig. 2, black line) indicate

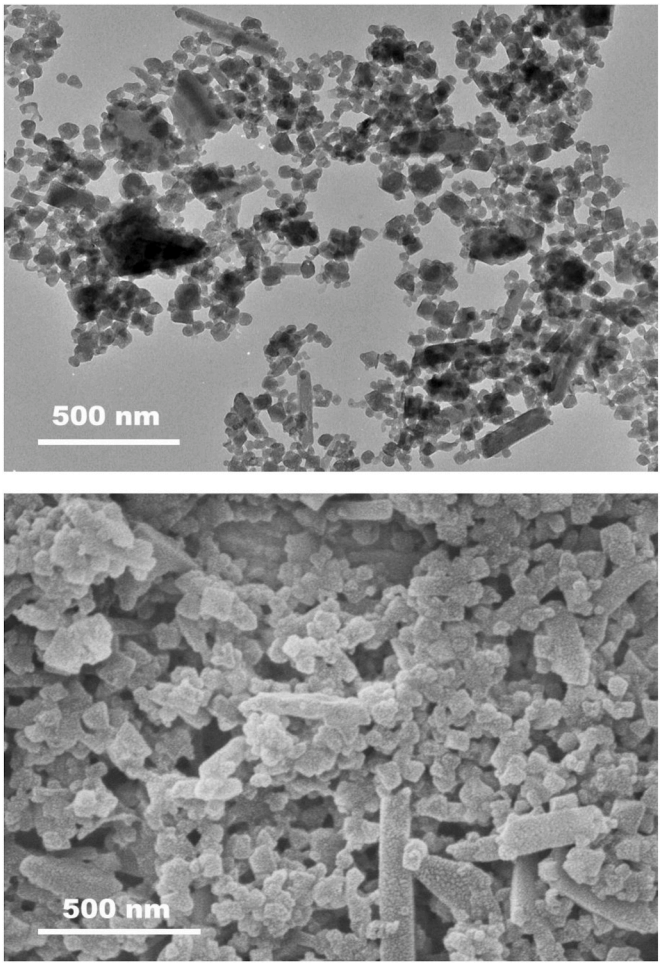

Fig. 1. Transmission electron microscopy (up) and scanning electron microscopy (down) images of concentrated Ti oxides (after removing iron oxides and silicates) in sample FTPZ.

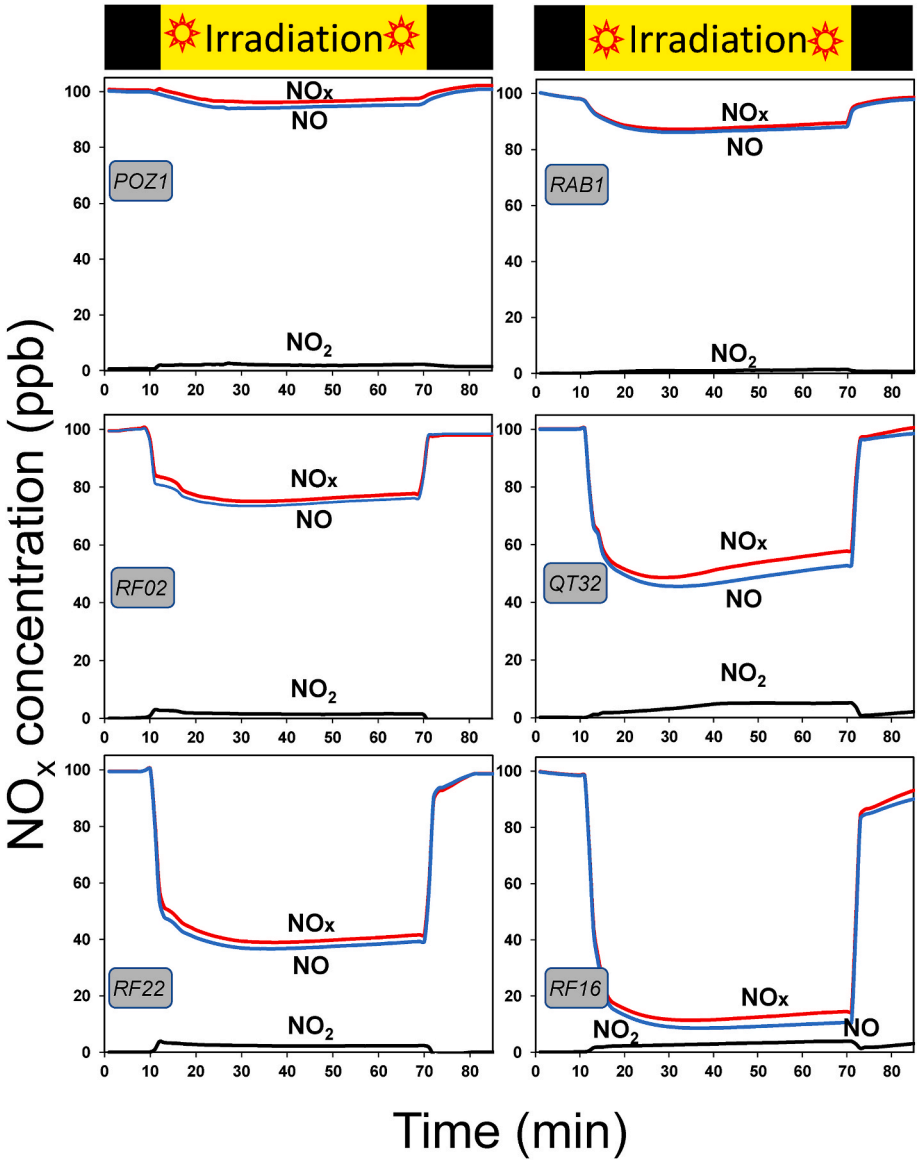

Fig. 2. Photocatalytic fixation of NO_x for selected soils. The concentrations of NO gas (blue line) flowing on the soil (at 20 °C) decreased abruptly when artificial sunlight (irradiance Vis/UV: 550/27 W m^{-2}) was switched on at min. 10. Then, for the next 60 min under irradiation, NO gas was seemingly oxidized to NO_2, but the small increase from background levels suggests that NO_2 (black line) was in turn consecutively transformed into NO_3^-. Loss of NO_x (NO + NO_2) (red line), which represents the amount of finally formed nitrate during the experiment, increased from quartzitic sandy soils (POZ1) to clayey and TiO_2 rich soils (RF16).

that it was in turn efficiently transformed into nitrate according to the following reactions (Laufs et al., 2010).

a) formation of pairs of electrons in the conduction band (e^-_{cb}) and holes in the valence band (h^+_{vb}) on the semiconductor TiO_2 from the soil caused by the UV irradiation:

$$TiO_2 + h\nu \rightarrow e^-_{cb} + h^+_{vb} \quad (2)$$

b) formation of reactive oxygen species ($^\bullet O_2^-$, $^\bullet HO_2$ and $^\bullet OH$) by consecutive reaction of the mobile charges with oxygen and water on the soil surface:

$$O_2 + e^-_{cb} \rightarrow {}^\bullet O_2^- \quad (3)$$

$$^\bullet O_2^- + H^+ \rightarrow {}^\bullet H\,O_2 \quad (4)$$

$$H_2O + h^+_{vb} \rightarrow H^+ + {}^\bullet O\,H \quad (5)$$

c) consecutive oxidation of NO to NO_2 and finally to nitrate according to the following reactions:

$$NO + {}^\bullet HO_2 \rightarrow NO_2 + {}^\bullet OH \quad (6)$$

$$NO_2 + {}^\bullet O\,H \rightarrow NO_3^- + H^+ \quad (7)$$

NO_2 is an intermediate of this reaction, which for the present soil samples does not significantly escape to the gas phase as was confirmed by the small concentrations detected. This is in stark contrast to other materials typically used for NO_x abatement. For example, in comparison to the commercial TiO_2 P25 (Degussa), which is slightly acidic (Bloh et al., 2014; Pashkova et al., 2022), the levels of NO_2 (considerably more toxic than NO) generated as a result of photocatalysis were very low for all the soils in this study, which gives soils a significant additional advantage as photocatalysts. Interestingly, it has been shown recently by Pastor et al. (2022) that layered double hydroxide De-NO_x photocatalysts also exhibit low NO_2 yields; this could be due to their ability to physically/chemically adsorb NO_2 on the mineral surface and, therefore, facilitate complete photocatalytic oxidation.

The low NO_2 formation and high total NO_x uptake (red line in Fig. 2), indicate that there was a fixation of NO_x as nitrate in soils, as previously reported (Barrón et al., 2020). The shape of the curves of NO_x uptake for the different soils was essentially similar from a qualitative perspective. However, quantitative differences were observed for some samples (Fig. 2). We calculated the photocatalytic fixation from the cumulative amount of NO_x removed from the gas flow, and estimated the theoretical nitrate generated considering gas flow rate, pressure, temperature, and reaction stoichiometry (Figure S6). The nitrate formed as a final product in selected samples is shown in Table S2. In order to calculate the balance of nitrate, organic matter and N in solution were removed from the samples before the experiments. Thus, we can assume that the measured nitrate after the laboratory experiments was generated only through photocatalytic reactions. In addition, we observed that the ratio of measured NO_3^-/estimated NO_3^- was in some cases as high as 3.3 (Table S2), indicating that other nitrogen sources could be responsible for this additional nitrate generation. The energy required to break the triple *N*–N bond in nitrogen (9.8 eV) is considerably higher than provided by photocatalysis mediated by TiO_2 (3.2 eV), which was justified by Density Functional Theory (Yuan et al., 2013). More recently, Pashkova et al. (2022) justified again the production of NO_3^- from a mixture of synthetic air through the photocatalysis of N_2 on TiO_2. Dhar et al. (1941) reported N_2 fixation as NO_3^- using sterile soils to which they added different carbon compounds. Al-Taani (2008) observed that the NO_3^- content of the sands was increased due to thermocatalytic N_2 fixation in soils from arid areas (deserts) subjected to temperatures of 70 °C in the dark. Therefore, the reasons for this higher NO_3^- amounts compared to stoichiometrically expected in our soils is not clearly elucidated and deserves further investigation.

3.3. Soil components influencing NO uptake

The uptake coefficients (γ_{geo}) (Pill et al., 2021) calculated for the different soils are displayed in Fig. 3 in decreasing order. They ranged from 0.1×10^{-6} for sandy soils and poor in titanium oxides (POZ1) to 6.4×10^{-5} in tropical soils (e.g. Ferralsols as RF10 or RF16 samples) with high clay, Al hydroxide and Fe and Ti oxides. It is also important to note that these soils with <5% Ti content had a photocatalytic efficiency comparable to pure P25 Degussa TiO_2 benchmark product also included in Fig. 3, which was tested under the same experimental conditions ($\gamma_{geo} = 10.9 \times 10^{-5}$).

Principal Component Analysis (PCA) for the 24 soils showed that the three first principal components explained 71.5% of the data variance, although here we only focus on the two most important (DIM 1 and DIM 2, Fig. 4A). The first component (40%) was explained by goethite, gibbsite, rutile, clay and anatase along with NO uptake, in one sense, and quartz and soil pH in the other. Quartz, concentrated in the coarser sand and silt fractions and transparent to UV–visible radiation, did not act as a photocatalyst and, consequently, there was a negative correlation to NO uptake (Fig. 4A and B). Other soil properties, e.g. surface area, total nitrogen, nitrate and organic matter content did not contribute to the photocatalytic efficiency of the soils either (Fig. 4A). However, total nitrogen and organic matter were the two most important contributors to the second principal component (17.2% of the total variance). In addition, after the removal of organic matter, a clear trend in the change of the photocatalytic efficiency was not observed (Figure S7). In some cases (62% out of the 24 soils), organic matter removal led to the dispersion of Fe oxides, which could more easily mask the photocatalytic reaction on anatase and rutile leading to lower activity, while in others (38%) the uptake of NO was enhanced when compared to the non-treated soils.

On the other hand, the soil components that better correlated with higher photocatalytic efficiencies were Al hydroxide (gibbsite), Fe oxides (goethite, but not hematite), Ti oxides (rutile and anatase) and clay content (Fig. 4B). However, these statistical results may lead to misinterpretation, as they may be due to a covariance effect, since it is

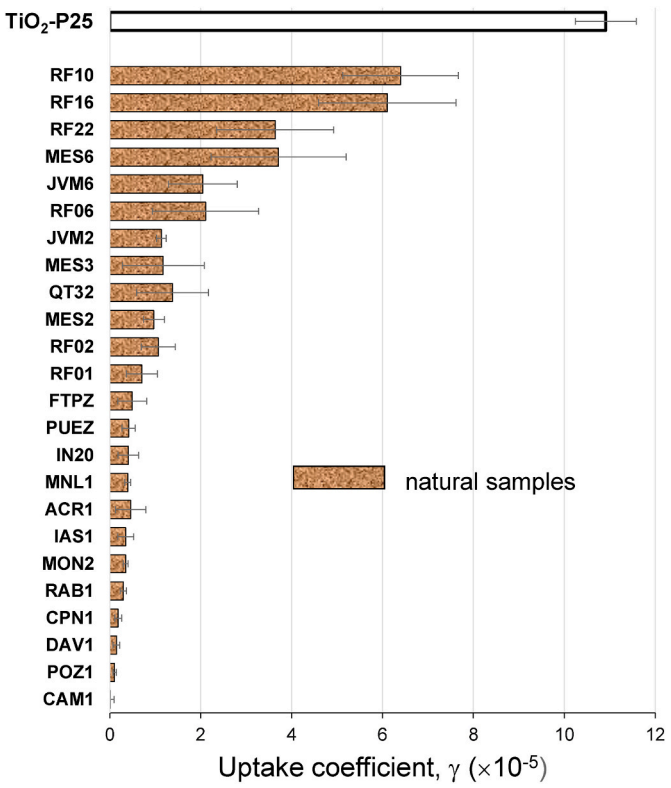

Fig. 3. Photocatalytic efficiency for natural samples. The NO uptake coefficient ranged from 0.1×10^{-6} for sandy soils and poor in titanium oxides (CAM1, POZ1) to 6.4×10^{-5} in tropical soils (e.g. Ferralsols as RF10 or RF16 samples) with high clay, Al hydroxide and Fe and Ti oxides. As a reference TiO_2 (Degussa P25) is shown applying an identical experimental protocol (irradiance, Vis/UV: 550/27 W m^{-2} at 20 °C).

expected that in the most weathered soils (tropical soils) Ti oxides are concentrated together with Al hydroxides (gibbsite) and Fe oxides. In fact, the removal of gibbsite (after NaOH treatment) from the most weathered or tropical soils did not result in a decrease of photocatalytic efficiency (Figure S8), which shows that this mineral does not influence the photocatalytic activity to the soils.

Furthermore, we also observed that the photocatalytic efficiency was drastically improved after selectively removing Fe oxides (Figure S9; grey bars). This shows that the presence of Fe oxides does not synergistically improve the photocatalytic efficiency of soils, in contrast to what has been reported for synthetic mixtures (Balbuena et al., 2015; Sugrañez et al., 2015). Indeed, Fe oxides seem to mask or hide the principal photocatalysts, anatase and rutile, by covering their surface and preventing radiation from triggering the photocatalytic mechanism. Hematite, with a higher pigmenting power than goethite (Barrón and Torrent, 1986) consequently had a greater effect than goethite.

Fig. 5 clearly shows that red soils, rich in hematite (MES3, RF02, RF01 and JVM2) are the ones that increase their photocatalytic efficiency the most once this pigment was selectively removed. These results discredit the interpretation proposed by Gan et al. (2021) attributing the photocatalytic mechanism of a red soil to the heterojunction of hematite with quartz, the latter mineral being moreover transparent to UV–visible radiation and, therefore, its involvement in photocatalysis is unlikely. On the other hand, it should be emphasized that selectively removing certain soil components could alter the soil properties, e.g. surface area or pH. Thus, while the activity after modification may absolutely not be representative for natural soils, this is still a useful tool to assess the impact of certain factors on photocatalysis. Furthermore, soils are extremely complex in mineralogy and physico-chemical properties. Hence, some of the factors with a positive

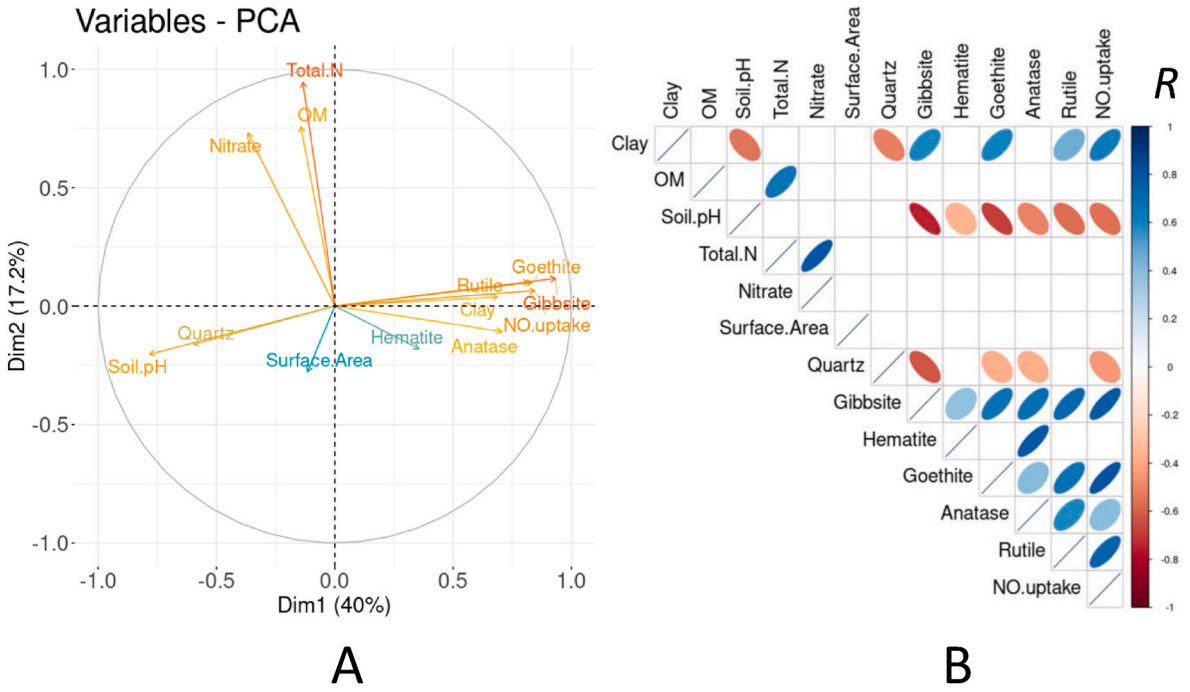

Fig. 4. Identification of potential soil components and properties involved in photocatalysis reactions. A: Principal Component Analysis (PCA) of the main variables for the 24 different soils used in the study. B: Correlation coefficients between the 13 variables used in the PCA.

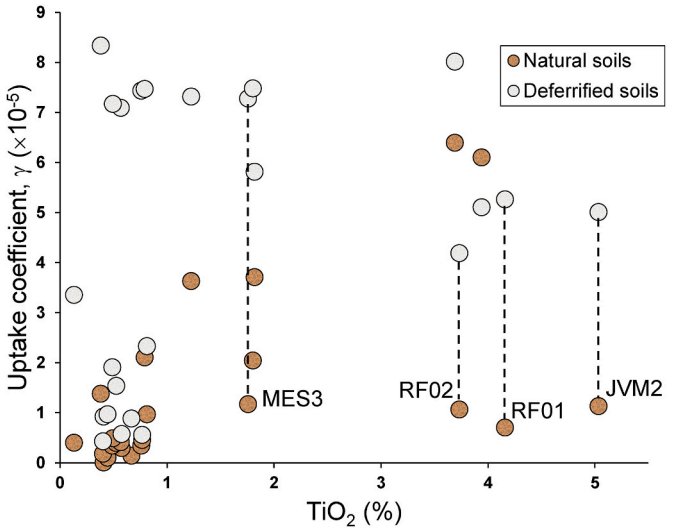

Fig. 5. Photocatalytic efficiency as a function of TiO_2. Red soils, rich in hematite (MES3, RF02, RF01 and JVM2) increase their photocatalytic efficiency (uptake coefficient) once their iron oxide pigments were selectively removed (grey) from the natural soil (orange). A small Ti oxide content of <1%, is enough to achieve a high photocatalytic efficiency.

or negative impact on NO uptake do not necessarily agree with what is known about photocatalysis on pure catalyst surfaces (e.g. on P25). This could be explained as co-variance of e.g., pH (with a negative correlation on NO uptake) with accessible TiO_2, the latter being the most determinant variable.

Regarding Ti oxides, a slightly better correlation of the NO uptake was observed for rutile than for anatase (Fig. 4B) in contrast to many synthetic compounds (Luttrell et al., 2015). As demonstrated here for soils for which Fe oxides were removed, even a small Ti oxide content of <1%, is enough to achieve a high photocatalytic efficiency (Fig. 4). This result is in line with the findings by Ndour et al. (2008) who reported that minor amounts of Ti oxides are sufficient for mineral dust in the atmosphere to undergo a significant photocatalytic reaction.

3.4. Geochemical implications and potential applications

The photocatalytic oxidation of NO_x observed in natural soils may help to generally better understand oxidation processes in soils and the stability of soil organic matter (and consequent contribution to C sequestration) in tropical and subtropical soils. Is there only an adsorption-complexation effect of humic compounds on the surface of Fe oxides, as suggested by Kirsten et al. (2021) or could these minerals also mask the effect of photocatalytic oxidation by Ti oxides, which are also relatively abundant in these soils? Similarly, the role of photocatalytic oxidation should be considered in the natural degradation of pesticides and other organic chemicals that pollute agricultural soils. The diversity of soils on a global scale and their different photocatalytic behavior in the oxidation and consequent abatement of NO_x means that the edaphic factor should be included in models of gas exchanges involved in the abiotic nitrogen cycling at the Earth's surface. Likewise, many of the chemical reactions in natural soils in which other N compounds participate, but also C, S, and different metals (Doane, 2017b), could be facilitated by Ti oxides and should be deeply studied in the future.

On the other hand, soils could also potentially be used as the basis of a more economical and sustainable alternative strategy for the mitigation of these pollutants, instead of the materials used now that are mainly synthetic Ti oxides (Wang et al., 2022; Herrmann, 2005). Also, some of the soils with high photocatalytic capacity, such as the tropical soils studied here, could be of potential use in the abatement of organic pollutants and pathogens of the water supplies for human consumption in many developing countries (ASDIS, 2023; Aguilar et al., 2023). Although the development of synthetic materials and their role in the degradation of NO_x and other pollutants such as volatile organic compounds, SO_2 and H_2S, among others, have been extensively reviewed (Tsang et al., 2019), natural materials containing TiO_2 have not yet been practically tested. The results shown here on NO_x abatement open a new alternative for further research on the photocatalytic power of soils.

Finally, the contribution of these abiotic reactions to the N cycle in terrestrial ecosystems, especially in arid and semiarid regions, should be elucidated. This knowledge could be useful to achieve a better understanding and even to enhance the sustainability of agriculture in terms of greenhouse gas and NO_x emissions, and potentially minimize the need of N fertilizers input, depending on climatic conditions, radiation, properties and mineralogy of soils and management. This study could also inspire further research into the development of "solar fertilizers" (Comer et al., 2019). Therefore, our work shows that in addition to lightning and root dwelling legumes, reactive nitrogen nutrients can be supplied to the soil photocatalytically from the atmosphere. In future, this mechanism could be exploited to actively fertilize soil from ambient pollution.

4. Conclusions

The presence of Ti oxides in soils, such as anatase and rutile, is the key to their photocatalytic behavior in the oxidation of NO_x. Their homogeneous distribution in soils and micrometric size associated with the clay and fine silt fraction means that, in some cases, high Ti oxides contents (>1%) are not necessary to exhibit high photocatalytic efficiency, that is comparable to synthetic pure Ti oxide. In tropical and subtropical soils, also rich in Fe oxides, these minerals did not exert a synergistic effect, but rather acted to mask the photocatalytic action of the Ti oxides. This was especially evident in the red-hematitic soils, since this Fe oxide has a higher pigmenting power than goethite, which is dominant in yellow soils.

Credit author statement

Antonio R Sánchez-Rodríguez: Conceptualisation, Funding acquisition, Investigation, Data curation. Writing – reviewing and editing. **Elena Gómez-Álvarez:** Investigation, Data curation. Writing – reviewing and editing Supervision. **José M Méndez***:* Methodology, Data curation. **Ute M Skiba***:* Supervision, reviewing. **Davey L Jones***:* Supervision, reviewing. **Dave R Chadwick:** Supervision, reviewing. **María C del Campillo***:* Funding acquisition, Writing – reviewing and editing. **Raphael BA Fernandes***:* Methodology. **Jörg Kleffmann***:* Data curation, Writing – reviewing and editing. **Vidal Barrón:** Conceptualisation, Writing – reviewing and editing.

Declaration of competing interest

The authors declare that they have no known competing financial interests or personal relationships that could have appeared to influence the work reported in this paper.

Data availability

Data will be made available on request.

Acknowledgments

We thank Professors B. Finlayson-Pitts (University of California, Irvine) and J. Williams (Max Planck Institute) for revision and constructive criticism of the manuscript. We are grateful to M. Mesquita and J.V. de Mello for providing soil samples. We also thank the Servicio Central de Apoyo a la Investigación (SCAI) and the Instituto Universitario de Nanoquímica Fina (IUNAN) of the University of Córdoba for technical support in using Transmission and Scanning electron microscope, X ray fluorescence and X ray diffraction. This study was funded by (i) Regional funds, Junta de Andalucía-PAIDI 2020, Project AbioNSoil (Ref. P18-RT-3086), and (ii) the Spanish State Research Agency through the Severo Ochoa and Maria de Maeztu Program for Centers and Units of Excellence in R&D (Ref. CEX 2019-000968-M). EGA also thanks the Spanish Ministry of Universities for a María Zambrano fellowship funded by the Spanish Ministry of Universities and European Union Next Generation Plan.

Appendix A. Supplementary data

Supplementary data to this article can be found online at https://doi.org/10.1016/j.chemosphere.2023.139576.

References

ASDIS, 2023. Advanced Solar Disinfection. A photocatalyst to accelerate the inactivation of waterborne pathogens in drinking water. https://asdis.org/en/home/.

Aguilar, S.D., Ramos, D.R., Santaballa, J.A., Canle, M., 2023. Preparation, characterization and testing of a bulky non-supported photocatalyst for water pollution abatement. Catal. Today 413–415, 113992. https://doi.org/10.1016/j.cattod.2022.12.023.

Al-Taani, A.A., 2008. Non-biological Fixation of Atmospheric Nitrogen to Nitrate on Titanium Dioxide and Desert Soil Surfaces. A dissertation in the University of Nevada.

Balbuena, J., Cruz-Yusta, M., Sánchez, L., 2015. Nanomaterials to combat NO_X pollution. J. Nanosci. Nanotechnol. 15, 6373–6385. https://doi.org/10.1166/jnn.2015.10871.

Banwart, S.A., Nikolaidis, N.P., Zhu, Y.G., Peacock, C.L., Sparks, D.L., 2019. Soil functions: connecting earth's critical zone. Annu. Rev. Earth Planet Sci. 47, 333–359. https://doi.org/10.1146/annurev-earth-063016-020544.

Barrón, V., Méndez, J.M., Balbuena, J., Cruz-Yusta, M., Sánchez, L., Giménez, C., Sacristán, D., González-Guzmán, A., Sánchez-Rodríguez, A.R., Skiba, U.M., Inda, A. V., Marques, J., Recio, J.M., Delgado, A., del Campillo, M.C., Torrent, J., 2020. Photochemical emission and fixation of NO_X gases in soils. Sci. Total Environ. 702 https://doi.org/10.1016/j.scitotenv.2019.134982.

Barrón, V., Torrent, J., 1986. Use of the Kubelka—munk theory to study the influence of iron oxides on soil colour. J. Soil Sci. 37 https://doi.org/10.1111/j.1365-2389.1986.tb00382.x.

Barrón, V., Torrent, J., 2013. Iron, Manganese and Aluminium Oxides and Oxyhydroxides. Eur. Mineral. Union Notes Mineral. 14, 297–336. https://doi.org/10.1180/EMU-notes.14.9.

Bloh, J.Z., Folli, A., Macphee, D.E., 2014. Photocatalytic NO_x abatement: why the selectivity matters. RSC Adv. 4, 45726–45734. https://doi.org/10.1039/c4ra07916g.

Bünemann, E.K., Bongiorno, G., Bai, Z., Creamer, R.E., De Deyn, G., de Goede, R., Fleskens, L., Geissen, V., Kuyper, T.W., Mäder, P., Pulleman, M., Sukkel, W., van Groenigen, J.W., Brussaard, L., 2018. Soil quality – a critical review. In: Soil Biol. Biochem. Elsevier Ltd May 1, pp. 105–125. https://doi.org/10.1016/j.soilbio.2018.01.030.

Comer, B.M., Fuentes, P., Dimkpa, C.O., Liu, Y.H., Fernandez, C.A., Arora, P., Realff, M., Singh, U., Hatzell, M.C., Medford, A.J., 2019. Prospects and challenges for solar fertilizers. Joule 3, 1578–1605. https://doi.org/10.1016/j.joule.2019.05.001.

Dhar, N., Seshacharyulu, E., Biswas, N., 1941. New aspects of nitrogen fixation and loss in soils. In: Proc. Natlional Inst. Sci. India, pp. 115–131. https://www.insa.nic.in/writereaddata/UpLoadedFiles/PINSA/Vol07_1941_2_Art02.pdf.

Doane, T.A., 2017a. The abiotic nitrogen cycle. ACS Earth Sp. Chem. 1, 411–421. https://doi.org/10.1021/acsearthspacechem.7b00059.

Doane, T.A., 2017b. A survey of photogeochemistry. Geochem. Trans. 18, 1–24. https://doi.org/10.1186/s12932-017-0039-y.

Fitzpatrick, R.W., Chittleborough, D.J., 2018. Titanium and zirconium minerals. Soil Mineral. with Environ. Appl. 7, 667–690. https://doi.org/10.2136/sssabookser7.c22.

Fitzpatrick, R.W., Le Roux, J., Schwertmann, U., 1978. Amorphous and crystalline titanium and iron-titanium oxides in synthetic preparations, at near ambient conditions, and in soil clays. Clay Clay Miner. 26, 189–201. https://doi.org/10.1346/ccmn.1978.0260302.

Fragoso, J., Pastor, A., Cruz-Yusta, M., Martin, F., de Miguel, G., Pavlovic, I., Sánchez, M., Sánchez, L., 2023. Graphene quantum dots/NiTi layered double hydroxide heterojunction as a highly efficient De-NOx photocatalyst with long persistent post-illumination action. Appl. Catal. B Environ. 322, 122115 https://doi.org/10.1016/j.apcatb.2022.122115.

Gan, Y., Abdellatif, H.R.S., Zhang, J., Wan, Y., Zeng, Q., Chen, J., Ni, J., Zhang, Y., E, S., Ni, C., 2021. Photocatalytic nitrogen-oxide conversion in red soil. J. Clean. Prod. 326, 129377 https://doi.org/10.1016/j.jclepro.2021.129377.

Gandolfo, A., Bartolomei, V., Gomez Alvarez, E., Tlili, S., Gligorovski, S., Kleffmann, J., Wortham, H., 2015. The effectiveness of indoor photocatalytic paints on NO_x and HONO levels. Appl. Catal. B Environ. 166–167, 84–90. https://doi.org/10.1016/j.apcatb.2014.11.011.

Gee, G.W., Bauder, J.W., 1986. Particle size analysis. In: Methods of Soil Analysis. Part 1. Physical and Mineralogical Methods. American Society of Agronomy, S.S.S. of A, Madison, pp. 383–411.

Georgiou, C.D., Sun, H.J., McKay, C.P., Grintzalis, K., Papapostolou, I., Zisimopoulos, D., Panagiotidis, K., Zhang, G., Koutsopoulou, E., Christidis, G.E., Margiolaki, I., 2015. Evidence for photochemical production of reactive oxygen species in desert soils. Nat. Commun. 6, 1–11. https://doi.org/10.1038/ncomms8100.

Guo, L., Chen, J., Luo, D., Liu, S., Lee, H.J., Motallebi, N., Fong, A., Deng, J., Rasool, Q.Z., Avise, J.C., Kuwayama, T., Croes, B.E., FitzGibbon, M., 2020. Assessment of nitrogen oxide emissions and san joaquin valley PM2.5 impacts from soils in California. J. Geophys. Res. Atmos. 125, 1–19. https://doi.org/10.1029/2020JD033304.

Herrmann, J.M., 2005. Heterogeneous photocatalysis: State of the art and present applications. Top. Catal. 34, 49–65. https://doi.org/10.1007/s11244-005-3788-2.
Kampf, N., Schwertmann, U., 1982. The 5-M-NaOH concentration treatment for iron oxides in soils. Clay Clay Miner. 30, 401–408. https://doi.org/10.1346/CCMN.1982.0300601.
Keyser, L.F., Moore, S.B., Leu, M.T., 1991. Surface reaction and pore diffusion in flow-tube reactors. J. Phys. Chem. 95, 5496–5502. https://pubs.acs.org/doi/10.1021/j100167a026.
Kirsten, M., Mikutta, R., Vogel, C., Thompson, A., Mueller, C.W., Kimaro, D.N., Bergsma, H.L.T., Feger, K.H., Kalbitz, K., 2021. Iron oxides and aluminous clays selectively control soil carbon storage and stability in the humid tropics. Sci. Rep. 11, 1–12. https://doi.org/10.1038/s41598-021-84777-7.
Klugg, H.P., Alexander, L.E., 1974. In: X-Ray Diffraction Procedures for Crystalline and Amorphous Materials. Sons, J. W., New York. In: https://www.wiley.com/en-us/X+Ray+Diffraction+Procedures%3A+For+Polycrystalline+and+Amorphous+Materials%2C+2nd+Edition-p-9780471493693.
Lal, R., 2020. Soil organic matter content and crop yield. J. Soil Water Conserv. 75, 27–32. https://doi.org/10.2489/JSWC.75.2.27A.
Laufs, S., Burgeth, G., Duttlinger, W., Kurtenbach, R., Maban, M., Thomas, C., Wiesen, P., Kleffmann, J., 2010. Conversion of nitrogen oxides on commercial photocatalytic dispersion paints. Atmos. Environ. 44, 2341–2349. https://doi.org/10.1016/j.atmosenv.2010.03.038.
Li, N., Wang, C., Zhang, K., Lv, H., Yuan, M., Bahnemann, D.W., 2022. Progress and prospects of photocatalytic conversion of low - concentration NO_x. Chin. J. Catal. 43, 2363–2387. https://doi.org/10.1016/S1872-2067(22)64139-1.
Luttrell, T., Halpegamage, S., Tao, J., Kramer, A., Sutter, E., Batzill, M., 2015. Why is anatase a better photocatalyst than rutile? - model studies on epitaxial TiO_2 films. Sci. Rep. 4, 1–8. https://doi.org/10.1038/srep04043.
Mehra, P.O., Jackson, M.L., 1960. Iron oxide removal from soils and clays by a dithionite-citrate system buffered with sodium bicarbonate. Clay Clay Miner. 7, 317–327.
Mulvaney, R.L., 1996. Nitrogen - inorganic forms. In: Sparks, D.L. (Ed.), Methods of Soil Analysis. Part 3. Chemical Methods. American Society of Agronomy, Soil Science Society of America, Madison, pp. 1123–1184. https://doi.org/10.2136/sssabookser5.3.c38.
Ndour, M., D'Anna, B., George, C., Ka, O., Balkanski, Y., Kleffmann, J., Stemmler, K., Ammann, M., 2008. Photoenhanced uptake of NO_2 on mineral dust: laboratory experiments and model simulations. Geophys. Res. Lett. 35, 1–5. https://doi.org/10.1029/2007GL032006.
Nelson, D.W., Sommers, L.E., 1982. Total carbon, organic carbon, and organic matter. In: Methods of Soil Analysis. Part 2. Chemical and Microbiological Properties. American Society of Agronomy, Soil Science Society of America, Madison, pp. 539–579.
Pashkova, A., Burek, B.O., Bloh, J., 2022. Sustainable nitrate production out of thin air: the photocatalytic oxidation of molecular nitrogen. Catal. Sci. Technol. 16–18. https://doi.org/10.1039/d2cy00350c.
Pastor, A., Chen, C., de Miguel, G., Martin, F., Cruz-Yusta, M., Buffet, J.C., O'Hare, D., Pavlovic, I., Sánchez, L., 2022. Aqueous miscible organic solvent treated NiTi layered double hydroxide De-NO_x photocatalysts. Chem. Eng. J. 429 https://doi.org/10.1016/j.cej.2021.132361.
Pilegaard, K., 2013. Processes regulating nitric oxide emissions from soils. Philos. Trans. R. Soc. B Biol. Sci. 368 https://doi.org/10.1098/rstb.2013.0126.
Pill, D., Wiesen, P., Kleffmann, J., 2021. Temperature dependencies of the degradation of NO, NO_2 and HONO on a photocatalytic dispersion paint. Phys. Chem. Chem. Phys. 23, 9418–9427. https://doi.org/10.1039/d1cp01157j.
Pradas del Real, A., Kaegi, R., Larue, C., de Nolf, W., Reyes-Herrera, J., Tucoulou, R., Findling, N., Salas-Colera, E., Sarret, G., 2018. Searching for relevant criteria to distinguish natural vs. anthropogenic TiO_2 nanoparticles in soils. Environ. Sci. Nano 5, 2853–2863.
Quirk, J.P., 1955. Significance of surface areas calculated from water sorption isotherms by use of the BET equation. Soil Sci. 80, 423–430.
R Core Team, 2020. R: A Language and Environment for Statistical Computing. R Foundation for Statistical Computing, Vienna, Austria. https://www.r-project.org/.
Raman, K.V., Jackson, M.L., 1965. Rutile and anatase determination in soils and sediments. Am. Mineral. 50, 1086–1092.
Russell, H.S., Frederickson, L.B., Hertel, O., Ellermann, T., Jensen, S.S., 2021. A review of photocatalytic materials for urban NO_x remediation. Catalysts 11, 1–45. https://doi.org/10.3390/catal11060675.
Scheinost, A.C., Chavernas, A., Barrón, V., Torrent, J., 1998. Use and limitations of second-derivative diffuse reflectance spectroscopy in the visible to near-infrared range to identify and quantify Fe oxide minerals in soils. Clay Clay Miner. 46, 528–536. https://doi.org/10.1346/CCMN.1998.0460506.
Sugrañez, R., Balbuena, J., Cruz-Yusta, M., Martín, F., Morales, J., Sánchez, L., 2015. Efficient behaviour of hematite towards the photocatalytic degradation of NOx gases. Appl. Catal. B Environ. 165, 529–536. https://doi.org/10.1016/j.apcatb.2014.10.025.
Torrent, J., Barrón, V., 1993. Laboratory Measurement of Soil Color: Theory and Practice. SSSA Special Publication (Soil Science Society of America.
Tsang, C.H.A., Li, K., Zeng, Y., Zhao, W., Zhang, T., Zhan, Y., Xie, R., Leung, D.Y.C., Huang, H., 2019. Titanium oxide based photocatalytic materials development and their role of in the air pollutants degradation: overview and forecast. Environ. Int. 125, 200–228. https://doi.org/10.1016/j.envint.2019.01.015.
Villena, G., Bejan, I., Kurtenbach, R., Wiesen, P., Kleffmann, J., 2012. Interferences of commercial NO_2 instruments in the urban atmosphere and in a smog chamber. Atmos. Meas. Tech. 5, 149–159. https://doi.org/10.5194/amt-5-149-2012.
Wang, Y., Torres, J., Meital, S., Carmo, M., Tao, H., Ribeiro, C., 2022. Photocatalytic materials applications for sustainable agriculture. Prog. Mater. Sci. 130.
Weil, R.R., Brady, N.C., 2016. The Nature and Properties of Soils. Pearson, 978-0133254488. https://www.pearson.com/en-us/subject-catalog/p/nature-and-properties-of-soils-the/P200000000825/9780137516933.
Whittig, L.D., Allardice, W.R., 1986. X-ray diffraction techniques. In: Klute, A. (Ed.), Methods of Soil Analysis. Part 1. Physical and Mineralogical Methods. American Society of Agronomy, Soil Science Society of America, Madison, pp. 331–363.
WRB, I.W.G., 2015. World Reference Base for Soil Resources 2014 (Rome).
Yuan, S.J., Chen, J.J., Lin, Z.Q., Li, W.W., Sheng, G.P., Yu, H.Q., 2013. Nitrate formation from atmospheric nitrogen and oxygen photocatalysed by nano-sized titanium dioxide. Nat. Commun. 4 https://doi.org/10.1038/ncomms3249.